An overview on the development and calibration of a 1D ejector model

Jan Van den Berghe

Environmental and Applied Fluid Dynamics Department, von Karman Institute for Fluid Dynamics, Belgium, jan.vandenberghe@vki.ac.be

Supervisor: Miguel Alfonso Mendez

Assistant Professor, Environmental and Applied Fluid Dynamics Department, von Karman Institute for Fluid Dynamics, Belgium, miguel.alfonso.mendez@vki.ac.be

University Supervisor: Yann Bartosiewicz

Professor, Institute of Mechanics, Materials, and Civil Engineering, Université catholique de Louvain, Belgium, yann.bartosiewicz@uclouvain.be

Abstract

We present a 1D ejector model with two streams which combines elements from existing models to reconcile pressure equalization, choking and shear. To this end, the compound choking theory is extended with a shear and friction force. Next, the model is calibrated on experimental and numerical data. Finally, we present a physics-constrained machine learning formalism to calibrate systems of ODEs with a neural network term.

Keywords: compound choking, physics-constrained machine learning, calibration with neural networks, adjoint method

1. Introduction

Ejectors are components to drive a flow without moving parts. They expand a primary fluid at high pressure through a nozzle which exhausts in a mixing chamber (cf. figure 1). A secondary flow is entrained into the resulting low pressure region through shear with the primary jet. The mixed flow recovers pressure in a diffuser and is choked in on-design operation. It becomes subsonic at higher back pressure in the so-called off-design regime and eventually reverses. The lack of moving parts makes ejectors robust devices, with applications in aeronautics, refrigeration, chemical industry and power generation [1].

Research on ejectors usually focuses on 2D/3D CFD [2–6] or 0D/1D modelling [7–15], which both require validation against experiments. Despite good accuracy of these methods, some phenomena remain unclear, particularly the choking mechanism of the combined primary and secondary jet (the so-called *compound* flow) [16]. Moreover, it can not easily be investigated without the appearance of shock trains at the exit of the primary nozzle (cf. figure 1). Such 2D phenomena complicate the development of 1D models which are inherently limited to an averaged representation. Such practical issues partially explain why 0D models are historically more popular. These low order models can be validated against mass flow rates, whereas 1D models *also* require local validation, for example the static pressure evolution in the mixing pipe. In other words, the extra local information comes at the cost of more complex calibration.

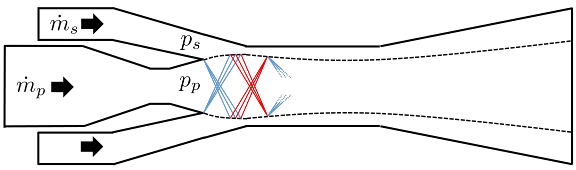

Figure 1: Schematic representation of an ejector. The primary jet exhausts at a static pressure p_p and is generally underexpanded ($p_p > p_s$), leading to a train of expansion waves (blue) and compression waves (red).

Notable contributions in 1D modelling were made by Clark [10] and Banasiak and Hafner [11], who proposed an ejector model consisting of two interacting 1D domains in the mixing pipe. The shock train at the exit of the primary nozzle is lumped into a 0D junction at the inlet of the mixing pipe. In [10], the authors consider the two streams as mass tubes which exchange momentum through shear. Their model is easily interpretable, but has not been validated locally. The predictions by [11] match well with local pressure measurements, but the model contains an unpractical number of closure parameters. In particular, the exchange of both mass *and* momentum complicates calibration and restricts the physical meaning of the dividing line between the streams, which is no longer a dividing *streamline* due to the mass transfer. Finally, neither of the models tackle on-design operation. An alternative approach was proposed by Del Valle et al. [12], which is based on potential flow and Prandtl-Meyer expansion theory. It recovers the dividing streamline that lets the static pressures equalize, but is restricted to isentropic and on-design operation.

These models illustrate the complex interaction between three concurrent phenomena in the mixing chamber: (1) equalization of the static pressure between the two jets, (2) momentum transfer through shear and wall friction and (3) choking of the compound flow. These phenomena are inherently 2/3D, so a 1D model requires additional closure terms to be calibrated against data. These terms can be considered as constants or, more interestingly, can be linked to state variables of the model. This makes the model more self-standing and thus reduces the need for ad hoc calibration. For example, a shear coefficient could depend on the Reynolds number in both streams.

This work proposes the first building blocks towards a 1D ejector model that tackles the three phenomena mentioned above and that is augmented by data-driven closure relations. These functional relations will be parametrized and learned with machine learning, e.g. with artificial neural networks (ANN). By training such a model on trusted experimental and numerical data, it bridges the gap between low-order models, CFD, and experiments, which constitutes the final goal of this work.

Several ingredients are required to reach this goal: firstly, a robust 1D model which works in multiple operating regimes (on-design, off-design and backflow). Secondly, we need numerical and experimental data for local verification and validation. Finally, we need calibration tools to learn the closure relations from data, which can be stated mathematically as a regression problem constrained by set of ODEs or PDEs. This work presents the progress on these three aspects in sections 2-4 respectively and closes with perspectives on future work in section 5.

2. A 1D ejector model

2.1. Adaptation of existing models

Model description.

The model proposed in this works combines the structure of [11] with the compound equations proposed in [10]. The structure is illustrated in figure 2: the inlets are modeled as 1D domains, which require a total pressure and total temperature as boundary condition and discharge in a 0D control volume. The static pressures of both streams equalize across this volume and enter two coupled 1D domains for the mixing pipe. The steady Euler equations are solved in each domain. In the mixing pipe, these are complemented by the assumption of equal static pressure in both streams [17] and the geometrical constraint on the cross-sections, cf. system (1). The assumption on the pressure addresses the degree of freedom of the dividing line: the conservation equations can be respected with a narrow primary and a wide secondary section or vice versa. Only a single dividing streamline respects the pressure constraint. The equations described above read:

$$\begin{cases} d_x\left(\rho_i A_i u_i\right) & = 0, \\ d_x\left(\rho_i A_i u_i^2\right) & = -A_i d_x p_i + F_i, \qquad i \in [p, s] \\ d_x\left(\rho_i A_i u_i h_{t,i}\right) & = 0, \end{cases}$$
$$\begin{cases} A_p + A_s & = A, \\ p_p & = p_s, \end{cases} \tag{1}$$

where x denotes the axial coordinate, ρ the density, A the cross-section, u the velocity, p the static pressure, F the external force, h_t the total specific enthalpy and the indices p and s denote the primary and secondary stream. The system is completed with a shear force, which has an equal but opposite effect on the streams, and a wall friction force in the secondary stream. These forces are parametrized with the friction coefficients f_{ps} and f_w:

$$F_p = -\frac{1}{2} f_{ps}\left(\rho_p u_p^2 - \rho_s u_s^2\right), \tag{2}$$

$$F_s = \frac{1}{2} f_{ps}\left(\rho_p u_p^2 - \rho_s u_s^2\right) - \frac{1}{2} f_w \rho_s u_s^2. \tag{3}$$

The concept of the compound equations above is appealing since there is no mass transfer between the two streams. The evolution of the primary cross-section in x thus takes the physical meaning of a dividing streamline in a 2D slice as in [10] and [12]. Furthermore, the same equations allow a formal description of choking, as discussed below in section

2.2. Finally, additional physical mechanisms can be added to system (1) if required. In this work, we focus on ideal gases and shear since it is the primary driving mechanism of entrainment. Friction is added as a first extension to account for losses. Other phenomena such as heat transfer are not included (yet).

The disadvantage of the compound equations consists of the assumption of equal static pressure. The shock trains in the mixing chamber (cf. figure 1) preclude using equations (1) directly at the exit of the primary nozzle. Instead, a pressure equalization mechanism can assimilate the shock cells in 1D [12] or the process is lumped in a 0D junction [11]. In this section, the second option is explored for its easier integration with a choking mechanism.

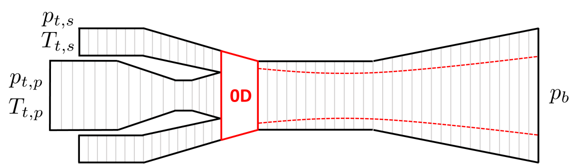

Figure 2: Schematic representation of the adapted 1D model. The primary and secondary inlets exhaust in a 0D control volume, across which the static pressures equalize. The mixing pipe is modelled as 2 streams which exchange momentum (cf. equations (1)-(3)).

Solution procedure.
The primary nozzle is always assumed to be choked and can therefore be solved individually. The secondary inlet can not be solved directly, since the mass flow rate is initially unknown. It can be calculated by first solving the junction. The operating regime is not known either, so the calculation initially assumes on-design operation. Practically, we assume the flow is choked at the exit of the 0D junction [15]. The proposed model distinguishes between the two streams in the mixing pipe, so the choking is enforced in the compound sense (cf. section 2.2 and [17; 16]).

The procedure for the junction is illustrated in figure 3 and iterates on the static pressure at the exit of junction until the flow becomes compound sonic in that section. Assuming no momentum exchange between the streams and with the wall, the total pressure and the total temperature are constant from inlet to outlet. With the guessed static pressure at the outlet, the Mach number in both sections can be calculated from the total and static pressure. The static temperature follows from the total temperature, and in turn the density and the velocity. The primary cross-sectional area follows from the mass flow rate (known from the choked nozzle) and the secondary area follows from the constraint on the geometry. The state at the outlet is then known completely, allowing to compute the compound Mach number M_{eq}. The on-design solution is found by iterating on the guessed static pressure until $M_{eq} = 1$.

At this point, the state at the inlet of the double flow passage is known, allowing to integrate equations (1) until the exit of the diffuser. It is important to note that a subsonic *and* a supersonic solution exist starting from the sonic boundary condition. In the first iteration we choose the subsonic solution, to obtain the highest back pressure $p_{b,crit}$ for which the ejector is choked. This value is required to verify if the assumption of on-design operation was correct. If the pressure imposed by the boundary condition is lower than $p_{b,crit}$, the flow will remain choked and the calculation is correct. The back pressure can be matched by computing the supersonic solution and by iterating on the position of a normal shock in the mixing pipe (as in a classic non-adapted 1D nozzle [18]). If the boundary pressure exceeds $p_{b,crit}$, the flow must remain subsonic and the ejector operates in off-design conditions. The procedure should then be repeated with a higher static pressure at the exit of the junction until the calculated back pressure matches the boundary condition.

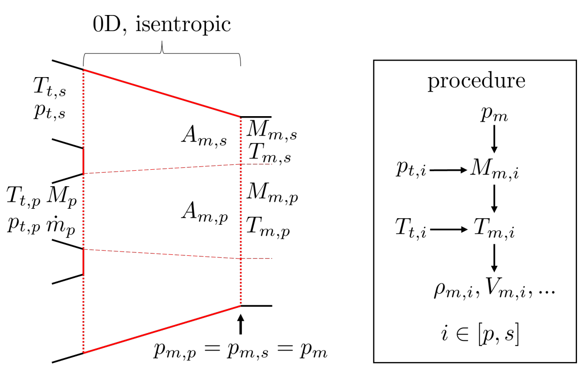

Figure 3: Solution procedure of the 0D junction. The displayed quantities at the inlet of the junction are known beforehand, those at the exit are calculated from a guessed static pressure p_m and through conservation equations.

2.2. *Extension of the compound flow theory*

The model described above is stated as a system of continuous equations, but these are singular in choked conditions. The equations are solved in practice by iterating on the static pressure in the next section $x+\Delta x$.

This is unfortunate, since a fully continuous formulation allows more efficient integration and a formal derivation of the adjoint problem, cf. section 4.

The system of equations (1) can be reformulated more compactly in terms of a single static pressure, two total pressures, two total temperatures and two cross-sections, from which all other quantities can be calculated. In this work, we focus on the equation for the static pressure since it is the source of the singularity in choked conditions. After some operations, the following equation can be obtained for the pressure gradient:

$$\frac{d_x p}{p} = \frac{1}{\beta}\Bigg(d_x A + \frac{f_{ps} l_{ps}}{2} \frac{\left(M_p^2 - M_s^2\right)^2}{M_p^2 M_s^2} - \frac{f_w l_w}{2}\left(1 + (\gamma - 1) M_s^2\right)\Bigg), \tag{4}$$

with

$$\beta = A_p \frac{1 - M_p^2}{\gamma M_p^2} + A_s \frac{1 - M_s^2}{\gamma M_s^2}, \tag{5}$$

where β denotes the compound choking indicator. The equation matches its single stream counterpart if $M_p = M_s = M$, in which case the denominator becomes $1 - M^2$. The *compound sonic* condition $\beta = 0$ is thus similar to a sonic condition of a single stream. Note that it is fulfilled if both Mach numbers equal 1, but can also be reached if one is subsonic and the other is supersonic. This explains why the secondary flow does not necessarily reach Mach 1 in on-design operation [16; 19]. The flow is *compound subsonic* if $\beta > 0$, and *compound supersonic* if $\beta < 0$.

Equation 4 is an extension of the original compound flow theory proposed by Bernstein [17], who did not include the effect of shear and friction. The second term represents the effect of shear and is positive by construction. As a result, shear tends to increase the static pressure in subsonic flow ($\beta > 0$). Similarly, the friction term is always negative, leading to a pressure decrease in subsonic flow and a pressure increase in supersonic flow (cf. Fanno flow [18]).

A choked section is thus characterized by a singularity in the pressure equation with $\beta = 0$. Nevertheless, the physical pressure gradient remains finite. Therefore, the numerator should also equal zero in a choked section. In absence of shear and friction, this leads to the condition that choking occurs in a throat. The positive shear term tends to push the area gradient to negative values in order to keep the numerator zero. In other words, shear pushes the choked section upstream towards a convergent section, which has been observed numerically [16]. Wall friction has the opposite effect and pushes the choked section into the diffuser. Note that the assumption in section 2.1 of choking at the throat of the mixing pipe is thus not strictly coherent with the current analysis! Resolving this discrepancy is a target for future work.

The pressure gradient can be computed in the singular point by applying de l'Hôpital‘s rule, which results in derivatives of the Mach number in the numerator and denominator and ultimately to a quadratic equation in terms of the pressure gradient. Its roots have opposite signs and correspond to the expected subsonic and supersonic solution. The derivation is too long to be included as an appendix, but is foreseen to appear as a technical note.

In summary, the framework in section 2.1 is a practical tool, but it is incoherent with the strict compound equations and needs to be solved iteratively. On the other hand, the set of equations in section 2.2 provide an analytical expression for the pressure gradient, but the assumption of equal static pressure is too restrictive to use directly in an ejector model due to the underexpanded primary jet. Combining these options, either with a 0D junction or with a pressure equalization mechanism, is the first priority in future work. The next section explores both options through calibration on experimental and numerical data.

3. Data collection and calibration with constant coefficients

3.1. Experimental facility

Figure 4 shows a sketch of the experimental facility. Compressed air is supplied on the top left. The inlet pressures are then regulated independently, allowing to set inlet pressure ratios $\Pi_2 = p_{t,s}/p_{t,p}$ between 0.2 and 1, with a maximal pressure of 5 bar. A 150 kW heater can heat one of the inlets up to a temperature of 200 °C. The flow settles through 2.5 m long straight pipes before passing through two vortex mass flow meters. The maximal achievable flow rate of the facility is 0.7 kg/s. Two flexible tubes allow to connect the heated inlet either to the primary or the secondary inlet of the ejector, which is located on the far right. Both inlets and the outlet are instrumented with four thermocouples and a pressure transducer connected to four pressure taps. With the measured mass flow rates and the known cross-section, these static quantities can be converted to their total counterparts to serve as boundary conditions in the numerical model. Finally, a manual valve at the diffuser exit allows to manipulate the back pressure.

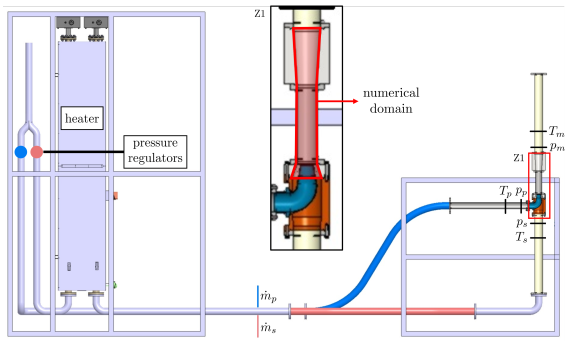

Figure 4: Schematic representation of the ejector facility at VKI.

A data point consists of two mass flow rates in given operating conditions. Their ratio is shown on figure 5 in function of the back pressure p_b and the total pressure at the secondary inlet p_{ts}, normalized by the primary total pressure p_{tp}. A higher inlet pressure ratio increases the entrainment ratio, while the back pressure determines the operating regime (on- and off-design). Increasing p_b beyond the shown points would lead to backflow, which is not considered in this work.

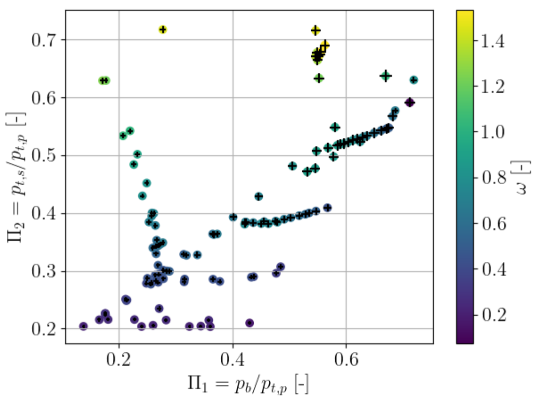

Figure 5: Experimentally obtained entrainment ratio $\omega = \dot{m}_s/\dot{m}_p$ in function of the back pressures ratio p_b/ptp and the inlet pressure ratio p_{ts}/p_{tp}. Entrainment increases with increasing secondary pressure and decreases with increasing back pressure p_b.

The model presented in section 2.1 contains 4 closure coefficients: the shear and wall friction coefficient f_{ps} and f_w in the mixing pipe, but also a friction coefficient in both inlet domains, which we denote with f_p and f_s. The primary mass flow rate is only affected by f_p since the primary nozzle is always choked in the considered conditions. The data then allow to calibrate one additional closure coefficient, which is why we lump all remaining losses in a total pressure loss $\Delta p_{t,s}$ at the secondary inlet, lowering the boundary condition of the total pressure with respect to the measured value. The shear coefficient f_{ps} is held constant at a default value of 0.01, which roughly corresponds to $\sigma = 13$ in [10].

The primary friction coefficient has been calibrated on the complete dataset, leading to $f_p = 0.0017$. On the other hand, the secondary pressure loss $\Delta p_{t,s}$ has been calibrated point by point since the secondary and mixed flow field change with the operating conditions. The evolution of $\Delta p_{t,s}$ is shown in function of the pressure ratios at the boundaries on figure 6. Higher losses are observed at lower back pressures p_b. A plausible explanation could be the higher flow rate in the on-design regime, but more local data is required to determine the source of the losses with more certainty. Note that $\Delta p_{t,s}$ evolves continuously in the plane of pressure ratios, independently of the inlet temperature ratio.

The corresponding mass flow rates are shown on figure 7 with the experimental uncertainty in x and the numerical uncertainty in y, which is obtained by propagating the uncertainties on the boundary conditions of the model. The predictions fall within an error margin of 10 %, indicated by the dashed lines. The numerical uncertainty is higher on the secondary mass flow rate compared to the primary due to the sensitivity to the back pressure in off-design operation.

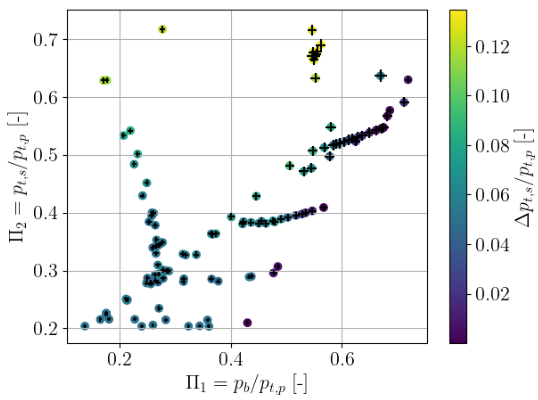

Figure 6: Result of the calibration of the secondary pressure loss $\Delta p_{t,s}$ in function of the back pressures ratio p_b/ptp and the inlet pressure ratio p_{ts}/p_{tp}. The loss correlates well with the entrainment ratio (cf. figure 5).

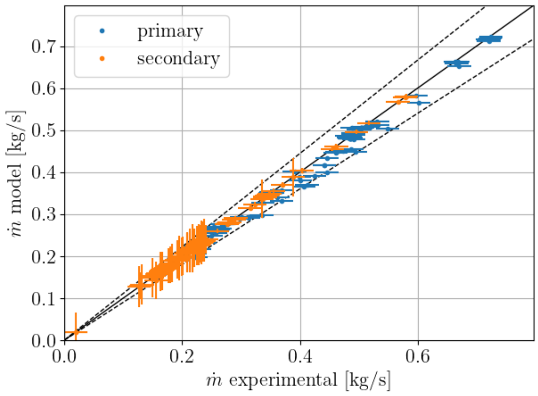

Figure 7: The predictions of the calibrated model fall within a 10 % error margin.

3.2. Numerical simulations

Axisymmetric RANS simulations are available on the same geometry as the experiments in the previous section [20]. In this work, we post-process these 2D simulations to produce 1D reference data for the model described in section 2. The first step consists of extracting the dividing streamline. Its radius at a certain position x is defined as follows:

$$\dot{m}_p(x) = \int_0^{r_{div}} \rho(x, r)u(x, r)\, 2\pi r\, dr. \tag{6}$$

Next, the dividing line is used to average the flow over the two streams with the following equations:

$$\hat{\rho}_i(x) = \frac{1}{A_i} \int_{A_i} \rho\, dA_i, \tag{7}$$

$$\hat{u}_i(x) = \frac{1}{\hat{\rho}_i A_i} \int_{A_i} \rho u\, dA_i, \tag{8}$$

$$\hat{e}_{ti}(x) = \frac{1}{\hat{\rho}_i A_i} \int_{A_i} \rho e_t\, dA_i, \tag{9}$$

where the hat $\hat{}$ denotes the averaged 1D variables and the integrals are to be carried out over the two cross-sections depending on the radius r_{div} of the dividing streamline. The choice to average the density is arbitrary, but the other two equations enforce that 1D mass flow rate and energy match their 2D counterparts [16].

Figure 8 shows the resulting dividing streamline for a simulation with a primary total pressure $p_{t,p}$ of 5 bar, a secondary total pressure $p_{t,s}$ of 1 bar and a back pressure p_b of 1 bar. The total temperatures are fixed at 293 K. The primary nozzle is underexpanded, leading to a shock train in the mixing chamber. This illustrates the need for a pressure equalization mechanism in the 1D model (cf. section 2). A second shock train appears in the diffuser to recompress the flow to the imposed static pressure at the outlet.

In contrast with the experiments, local data is now abundantly available, including the evolution of the primary cross-section. The procedure is split in two regions. In the first, the cross-sections of the streams are copied from the CFD from the exit of the primary nozzle until the static pressures equalize. Downstream, the cross-sections are calculated with the compound flow equations (cf. section 2). The on-design procedure assumes so-called Fabri-choking [8], which states that the secondary stream becomes sonic in its minimal cross-section. The first step thus consists of finding the minimal cross-section of the secondary stream, where $M_s = 1$ is imposed. Next, the total pressure is defined in the same section such that the mass flow rate matches the CFD (which remains the only free variable with the total temperature from the inlet, the area from the CFD and the unitary Mach number). In the same section, the primary Mach number and total pressure are tuned to match the CFD as closely as possible. This provides a starting point for integrating the conservation equations upstream to the inlets and downstream until the static pressures equalize.

From there on, the continuous compound equations from section 2.2 are integrated to a given coordinate where a shock is introduced. The flow remains supersonic because it was already compound supersonic in the choked section ($M_p > 1$ and $M_s = 1$). The shock is solved with the iterative procedure from section 2.1 with the additional requirement that the flow becomes subsonic. Afterwards, the compound equations are integrated once more until the exit of the domain.

Figure 9 shows the calibrated result on the post-processed CFD simulation from figure 8. Through trial and error, the wall friction coefficient is held constant throughout, with a final value of 0.002 and the shear coefficient is piece-wise constant, equaling 0.015 in the variable pressure region, 0.002 from the point where the pressure equalize to the shock and 0.010 downstream of the shock. The effect of the operating conditions on these closure coefficients is a target for future work. For now, it suffices to conclude that the 1D formulation is capable of accurately representing the internal flow field of an ejector in this specific operating point. Naturally, it can not reproduce the oscillations due the 2D shock trains, but the approximation with the normal shock allows to match the full state at the exit of the domain, as was observed earlier on integral quantities in transient conditions [15].

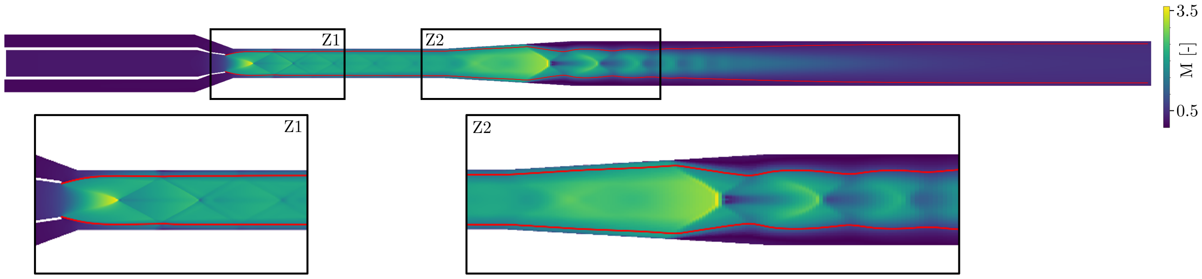

Figure 8: Mirrored Mach number field of a 2D simulation on an axisymmetric ejector with a primary inlet pressure of 5 bar, a secondary inlet pressure of 1 bar and a back pressure of 1 bar. The primary nozzle is underexpanded and the ejector operates in the on-design regime, leading to shock trains in the mixing chamber (zoom 1) and in the diffuser (zoom 2). The red line indicates the dividing streamline obtained in post-processing (cf. equation (6)).

4. Calibration with the adjoint method and artificial neural networks

4.1. Methodology

The ejector model described in section 2 consists of a set of ODEs with closure terms. It has been found in section 3 that the closure coefficients should vary in x. The ultimate goal is to find closure relations not in function of space, but of the local solution, e.g., pressures and velocities. This paradigm can be formalized as follows:

$$\begin{cases} d_t\boldsymbol{u} = f(\boldsymbol{u}, t, \boldsymbol{p}) \\ \boldsymbol{p} = g(\boldsymbol{u}, t; \boldsymbol{w}) \end{cases} \tag{10}$$

where $\boldsymbol{u} \in \mathbb{R}^{n_u}$ denotes the state vector, t denotes time (or space in steady 1D models), $\boldsymbol{p} \in \mathbb{R}^{n_p}$ denotes the vector of n_p closure parameters, which depend on the state, time and a set of weights $\boldsymbol{w} \in \mathbb{R}^{n_w}$ through the function g. The function g is thus the closure relation to be inferred from data, and is embodied by a regressor such as an artificial neural network (ANN). This approach has been used successfully on a Poisson equation [21] and later in turbulence modelling [22–25]. The calibration problem is solved by a set of weights that minimize a cost function of the following form:

$$J(\boldsymbol{w}) = \int_0^T e(\boldsymbol{u}, \tilde{\boldsymbol{u}})dt \tag{11}$$

where e can be any function that penalizes the mismatch between the numerical solution $\boldsymbol{u}$ and given data $\tilde{\boldsymbol{u}}$. Analytically calculating its gradient $d_{\boldsymbol{w}}J = d_{\boldsymbol{u}}J\, d_{\boldsymbol{p}}\boldsymbol{u}\, d_{\boldsymbol{w}}g$ is challenging because it is linked to the system of ODEs (10).

A brute force solution is to use finite differences, which implies solving the system (10) $n_w + 1$ times. This approach is infeasible for neural networks with thousands of weights. The adjoint method provides an alternative, which requires solving the following adjoint system of ODEs *once* and backwards in time (cf. [26] for a tutorial):

$$\dot{\boldsymbol{\lambda}} = d_{\boldsymbol{u}}e - \boldsymbol{\lambda}(\partial_{\boldsymbol{u}}f + \partial_{\boldsymbol{p}}f\, \partial_{\boldsymbol{u}}\boldsymbol{p}) \tag{12}$$

where $\boldsymbol{\lambda} \in \mathbb{R}^{n_u}$ denotes the adjoint state. This equation can be derived by augmenting the cost function (11) with a Lagrangian multiplier $\boldsymbol{\lambda}$ followed by the system of equations (10). By choosing the adjoint variables such that they respect the adjoint equation, the final expression for the gradient of the cost simplifies to the following equation:

$$d_{\boldsymbol{w}}J = -\int_0^T \boldsymbol{\lambda}\, \partial_{\boldsymbol{p}}f\, \partial_{\boldsymbol{w}}\boldsymbol{p}\, dt \tag{13}$$

In summary, the troublesome Jacobian of the solution with respect to the weights ($d_{\boldsymbol{w}}\boldsymbol{u}$) is avoided and replaced by an adjoint system of linear (!) equations, which require Jacobians that can be calculated from the definition of the original system of equations (10). In case the closure relation g is defined by a neural network, the Jacobians $\partial_{\boldsymbol{u}}\boldsymbol{p}$ and $\partial_{\boldsymbol{w}}\boldsymbol{p}$ can be computed through backpropagation [27].

4.2. Test case: Burgers' equation

We use a non-linear advection equation as test case:

$$\begin{cases} \partial_t u + a\partial_x u = 0 \\ a = g(u; \boldsymbol{w}) \end{cases} \tag{14}$$

where the advection speed a is prescribed by a neural network with input u and weights $\boldsymbol{w}$. This PDE becomes a system of ODEs after discretizing the space derivative. For simplicity, a first order upwind scheme is used for both space and time.

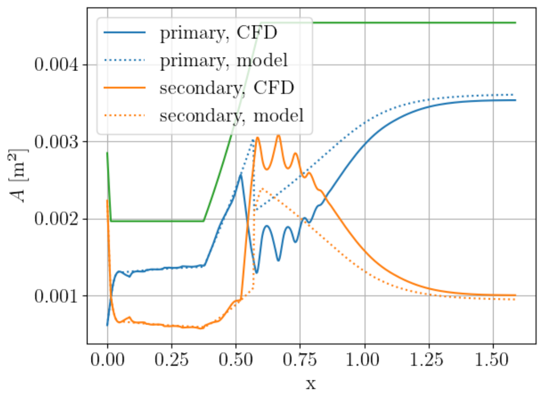

(a) Area

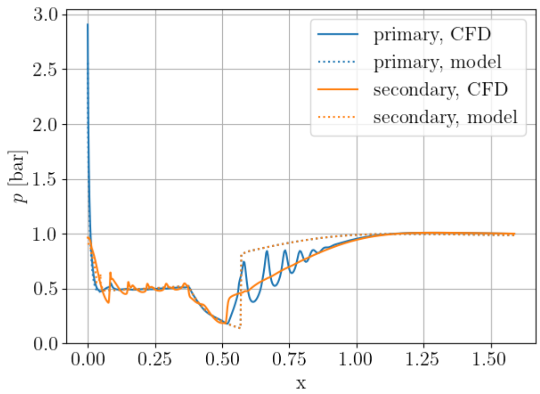

(b) Static pressure

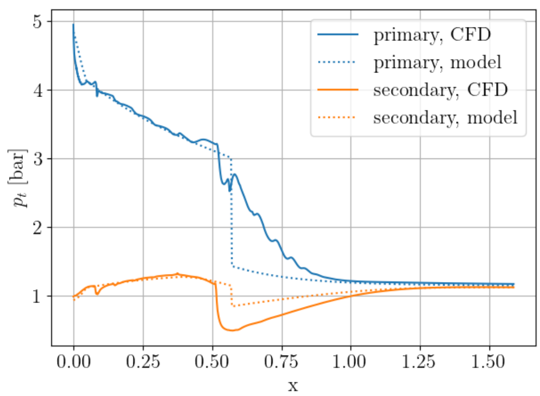

(c) Total pressure

Figure 9: Assimilation of the CFD simulation in figure 8, which was post-processed with equations (7) - (9). The result is obtained through calibration of the shear and the wall friction coefficients.

The neural network contains two hidden layers with ten nodes and ELU activation functions [28]. The output node has a sigmoid activation function to force the output in the range [0,1], to avoid stability issues with a reference speed of 1 and a CFL number of 0.8. The initial condition and the reference solution read:

$$\begin{cases} u_0(x) & = 0.6 + 0.3\sin(2\pi x) \\ a_{ref} & = 0.5 + 0.4\sin(2\pi u) \end{cases} \tag{15}$$

The cost function is the summed square error at the final time of 0.5 seconds. Figure 10 shows the solution (left) and the closure relation predicted by the neural network (right) as the training progresses. After ten iterations the neural network has learned to lower the advection speeds at high values of u. The main contribution to the cost at the initial time is indeed an overshoot of the peak between $x = 0.1$ and $x = 0.5$. The algorithm converges after 141 iterations. Although the data contains no noise and the function is well-behaved, it remains remarkable that the neural network manages to learn a function indirectly through the integration of a physical and adjoint equation.

5. Conclusion

In this work, we presented a 1D model which combines the ideas of three existing models to address the complex interaction between pressure equalization, choking and shear. To this end, the compound choking theory has been extended to include shear and friction forces. These equations show a discrepancy between the adapted model with the 0D junction and the analytical equations. Reconciling both options is a primary target in future work.

In parallel, experimental and numerical data have been collected for validation. The data cover all operating regimes of a single ejector. Other geometries can be considered in the future, but are not the main priority. The calibration on *global* experimental data does not allow to localize the losses in the secondary stream, but provides interpretable results in terms of pressure ratios. The calibration on CFD proves that a 1D formulation can also *locally* assimilate the flow field. Understanding the effect of the operating conditions on the calibration is an important future target.

Finally, we proposed a general framework for the adjoint-based calibration of ODE models with an ANN closure term. A non-linear advection equation was used as a proof of concept. A final target is to apply the method on the closure coefficients of the 1D ejector model, which first requires a fully continuous formulation.

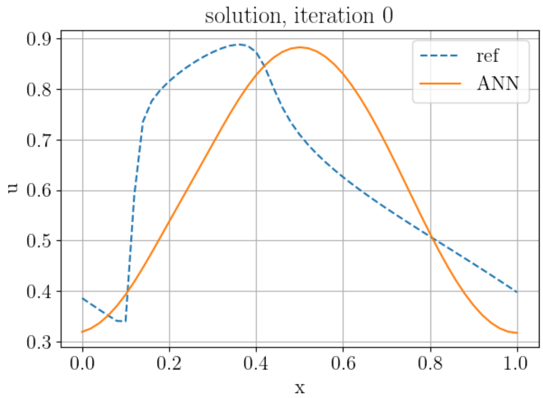

(a) Solution at iteration 0

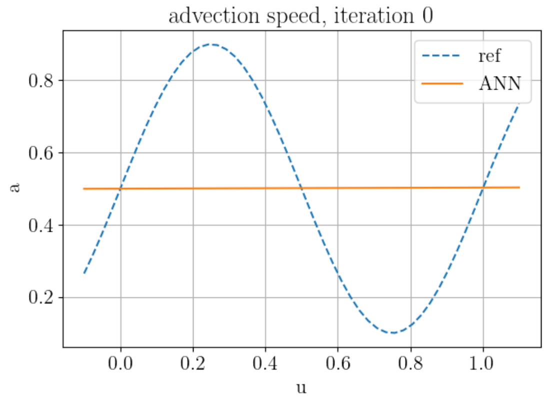

(b) Advection speed at iteration 0

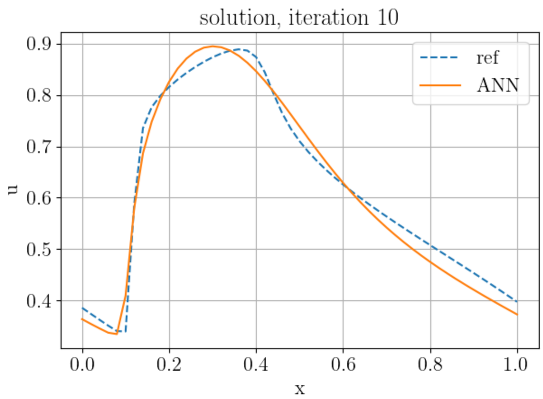

(c) Solution at iteration 10

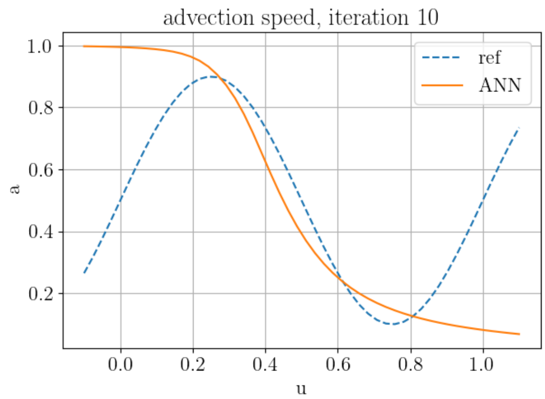

(d) Advection speed at iteration 10

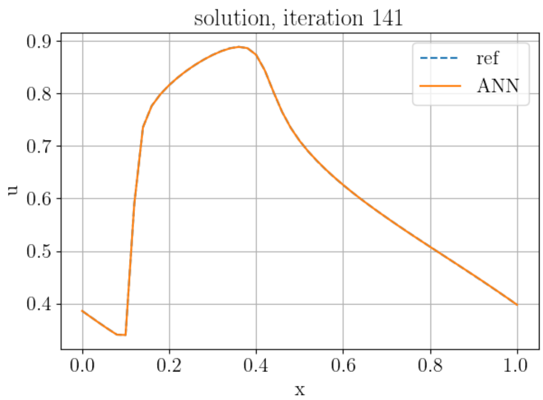

(e) Solution at iteration 141

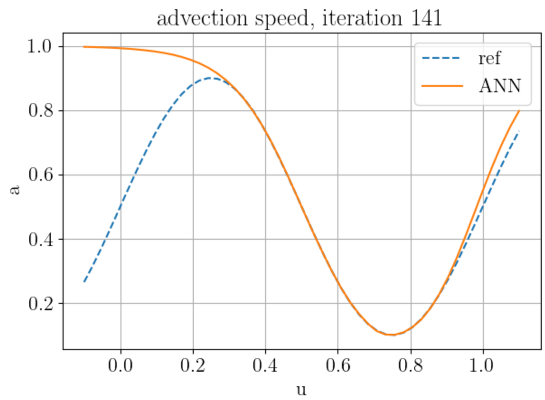

(f) Advection speed at iteration 141

Figure 10: Training history (top-bottom) of a non-linear advection equation where the speed (right) is prescribed by a neural network (cf. equation (14)). The error on the solution at the final time step (left) is penalized through a cost function, which is minimized with an adjoint method for the enhanced physical system (cf. equations (10) to (13)). The network manages to learn a sinusoidal function indirectly through the physical system.

Acknowledgments

J. Van den Berghe is supported by a F.R.S.-FNRS FRIA grant and gratefully acknowledges Mathieu Delsipee for the experiments and Dr. Jagadish Babu Vemula for the CFD simulations.

This project has received funding from the Clean Sky 2 Joint Undertaking (JU) under grant agreement No 101008100. The JU receives support from the European Union's Horizon 2020 research and innovation programme and the Clean Sky 2 JU members other than the Union.

Horizon 2020 European Union Funding for Research & Innovation

Clean Sky 2

Disclaimer: The contents presented in this article reflect only the author's point of view: the authors and Clean Sky JU are not responsible for any use that may be made of the information it contains.

References

[1] Z. Aidoun, K. Ameur, M. Falsafioon, M. Badache, Current advances in ejector modeling, experimentation and applications for refrigeration and heat pumps. part 1: Single-phase ejectors, Inventions 4 (1) (2019) 15.

[2] Y. Bartosiewicz, Z. Aidoun, P. Desevaux, Y. Mercadier, Numerical and experimental investigations on supersonic ejectors, International Journal of Heat and Fluid Flow 26 (1) (2005) 56–70. doi:10.1016/j.ijheatfluidflow.2004.07.003.

[3] A. Hemidi, F. Henry, S. Leclaire, J.-M. Seynhaeve, Y. Bartosiewicz, Cfd analysis of a supersonic air ejector. part i: Experimental validation of single-phase and two-phase operation, Applied Thermal Engineering 29 (8) (2009) 1523–1531. doi:10.1016/j.applthermaleng.2008.07.003.

[4] F. Mazzelli, A. B. Little, S. Garimella, Y. Bartosiewicz, Computational and experimental analysis of supersonic air ejector: Turbulence modeling and assessment of 3d effects, International Journal of Heat and Fluid Flow 56 (2015) 305–316. doi:10.1016/j.ijheatfluidflow.2015.08.003.

[5] O. Lamberts, P. Chatelain, Y. Bartosiewicz, New methods for analyzing transport phenomena in supersonic ejectors, International Journal of Heat and Fluid Flow 64 (2017) 23–40. doi:10.1016/j.ijheatfluidflow.2017.01.009.

[6] O. Lamberts, P. Chatelain, Y. Bartosiewicz, Numerical and experimental evidence of the fabri-choking in a supersonic ejector, International Journal of Heat and Fluid Flow 69 (2018) 194–209. doi:10.1016/j.ijheatfluidflow.2018.01.002.

[7] J. H. Keenan, E. P. Neumann, A Simple Air Ejector, Journal of Applied Mechanics 9 (2) (1942) A75–A81. doi:10.1115/1.4009187.

[8] J. Fabri, R. Siestrunck, Supersonic air ejectors, Advances in Applied Mechanics 5 (1958) 1–34.

[9] I. Eames, S. Aphornratana, H. Haider, A theoretical and experimental study of a small-scale steam jet refrigerator, International journal of refrigeration 18 (6) (1995) 378–386.

[10] L. Clark, Application of compound flow analysis to supersonic ejector-mixer performance prediction, in: 33rd Aerospace Sciences Meeting and Exhibit, 1995, p. 645.

[11] K. Banasiak, A. Hafner, 1d computational model of a two-phase r744 ejector for expansion work recovery, International Journal of Thermal Sciences 50 (11) (2011) 2235–2247. doi:10.1016/j.ijthermalsci.2011.06.007.

[12] J. G. del Valle, J. M. S. Jabardo, F. C. Ruiz, J. S. J. Alonso, A one dimensional model for the determination of an ejector entrainment ratio, International Journal of Refrigeration 35 (4) (2012) 772–784.

[13] W. Chen, M. Liu, D. Chong, J. Yan, A. B. Little, Y. Bartosiewicz, A 1d model to predict ejector performance at critical and sub-critical operational regimes, International Journal of Refrigeration 36 (6) (2013) 1750 – 1761. doi:10.1016/j.ijrefrig.2013.04.009.

[14] A. Metsue, R. Debroeyer, S. Poncet, Y. Bartosiewicz, An improved thermodynamic model for supersonic real-gas ejectors using the compound-choking theory, Energy (2021) 121856doi:10.1016/j.energy.2021.121856.

[15] J. Van den Berghe, B. R. Dias, Y. Bartosiewicz, M. A. Mendez, A 1d model for the unsteady gas dynamics of ejectors, Energy 267 (2023) 126551.

[16] O. Lamberts, P. Chatelain, N. Bourgeois, Y. Bartosiewicz, The compound-choking theory as an explanation of the entrainment limitation in supersonic ejectors, Energy 158 (2018) 524–536. doi:10.1016/j.energy.2018.06.036.

[17] A. Bernstein, W. Heiser, C. Hevenor, Compound-compressible nozzle flow.

[18] A. H. Shapiro, The dynamics and thermodynamics of compressible fluid flow, New York: Ronald Press.

[19] S. Croquer, Y. Fang, A. Metsue, Y. Bartosiewicz, S. Poncet, Compound-choking theory for supersonic ejectors working with real gas, Energy 227 (2021) 120396. doi:10.1016/j.energy.2021.120396.

[20] E. Schillaci, C. Oliet Casasayas, J. B. Vemula, M. Duponcheel, Y. Bartosiewicz, P. Planquart, Air ejector analysis in normal and abnormal modes, oriented to control purposes in aircraft systems, in: 9th European Conference for Aeronautics and Space Sciences (EUCASS), European Conference for AeroSpace Sciences (EUCASS), 2022, pp. 1–12.

[21] R. T. Chen, Y. Rubanova, J. Bettencourt, D. K. Duvenaud, Neural ordinary differential equations, Advances in neural information processing systems 31.

[22] J. R. Holland, J. D. Baeder, K. Duraisamy, Field inversion and machine learning with embedded neural networks: Physics-consistent neural network training, in: AIAA Aviation 2019 Forum, 2019, p. 3200.

[23] J. Sirignano, J. F. MacArt, J. B. Freund, Dpm: A deep learning pde augmentation method with application to large-eddy simulation, Journal of Computational Physics 423 (2020) 109811.

[24] J. Sirignano, J. MacArt, K. Spiliopoulos, Pde-constrained models with neural network terms: optimization and global convergence, arXiv preprint arXiv:2105.08633.

[25] J. F. MacArt, J. Sirignano, J. B. Freund, Embedded training of neural-network subgrid-scale turbulence models, Physical Review Fluids 6 (5) (2021) 050502.

[26] A. M. Bradley, Pde-constrained optimization and the adjoint method. 2019, URL https://cs. stanford. edu/˜ ambrad/adjoint_tutorial. pdf.

[27] D. E. Rumelhart, J. L. McClelland, Parallel Distributed Processing: Explorations in the Microstructure of Cognition: Foundations, MIT PRess, 1989.

[28] A. Géron, Hands-on Machine Learning with Scikit-Learn, Keras, and TensorFlow, 2nd Edition, O'Reilly, 2019.